

Leaving the Valley: Charting the Energy Landscape of Metal/Organic Interfaces via Machine Learning

Michael Scherbela, Lukas Hörmann, Veronika Obersteiner, and Oliver T. Hofmann.

*Institute of Solid State Physics, NAWI Graz, Graz University of Technology,
Petersgasse 16, 8010 Graz, Austria*

The rich polymorphism exhibited by inorganic/organic interfaces is a major challenge for materials design. In this work we present a method to efficiently explore the potential energy surface and predict the formation energies of polymorphs and defects. This is achieved by training a machine learning model on a list only 100 candidate structures that are evaluated via dispersion-corrected Density Functional Theory (DFT) calculations. We demonstrate the power of this approach for tetracyanoethylene on Ag(100) and explain the anisotropic ordering that is observed experimentally.

Introduction. Without knowing the atomistic structure of not yet synthesized materials, little can be said about their properties. This is a particular problem in organic-based applications, such as organic electronics, where the critical parameters such as electrical conductivity¹ and injection barriers² are strongly affected by polymorphism. Theoretical polymorph prediction is therefore a crucial step towards computational material design. However, currently most polymorph prediction methods are designed for isolated molecules³ or compact bulk systems.^{4,5} Only few approaches deal with interfaces, and there, with few notable exceptions⁶, the target is usually the geometry of isolated adsorbates rather than the polymorphism of extended monolayers.⁷⁻⁹

For organic monolayers, often several thousand potential local minima (corresponding to different polymorphs) exist. In practice, the small energy differences between them lead to rich polymorphism and high defect concentrations.¹⁰ Very often, structures with several inequivalent molecules^{11,12} are formed. For computational structure prediction, this leads to a huge dilemma: While the small energy differences require employing highly-accurate first-principle methods¹³, the large unit cells limit their applicability. This is because the large unit cells render each energy evaluation prohibitively expensive, while at the same time, the many degrees of freedom lead to a “combinatorial explosion” of the number of possible structures. Established stochastic methods can therefore only ever explore a tiny fraction of the vast configurational space, potentially missing the ground state structure and giving no systematic overview over possible polymorphs and corresponding defects.

In this contribution, we demonstrate how such an overview can be obtained using a quasi-deterministic, machine-learning based approach. Our approach requires as few as 100 DFT calculations, allowing us to

chart the polymorph landscape at affordable cost. Exemplarily applying our approach to TCNE adsorbed on Ag(100), we explain why it forms well-ordered lines in one crystallographic direction, while the other direction exhibits a large defect propensity.

Predicting the Potential Energy Surface. We obtain an exhaustive overview over the potential energy surface in three steps: First, we discretize the PES to build a large, exhaustive list of polymorph candidates. Secondly, we define a model that assigns energies to all polymorph candidates. Finally, we train this model using DFT and use it to rank all polymorph candidates.

To create a list of polymorph candidates we use the SAMPLE approach,¹⁴ which is developed for commensurate interfaces where the molecule-substrate interaction dominates over the intermolecular interactions: There, we first determine the geometries that a single, isolated molecule would adopt on the surface using traditional, local geometry optimization from different initial positions and orientations. For this work, all calculations were performed using the FHI-aims¹⁵ code package with the PBE¹⁶ exchange-correlation functional. Dispersion forces were accounted for using the Tkatchenko-Scheffler¹⁷ method with the surface parametrization.¹⁸ This method has been shown to yield reliable adsorption geometries¹⁹, energies¹⁸, and electronic structures²⁰. Further computational details are given in the Supporting Information.

For the example of TCNE/Ag(100) we find that the molecule adopts one of five possible adsorption sites, which are depicted in Fig. 1a. We note that four of these structures (A-C and E in Fig. 1a) were previously reported in a different computational study²¹, whereas D was not listed there. Conversely, we find two energetically higher-lying geometries reported in ref.²¹ not to be stable minimum geometries with our methodology.

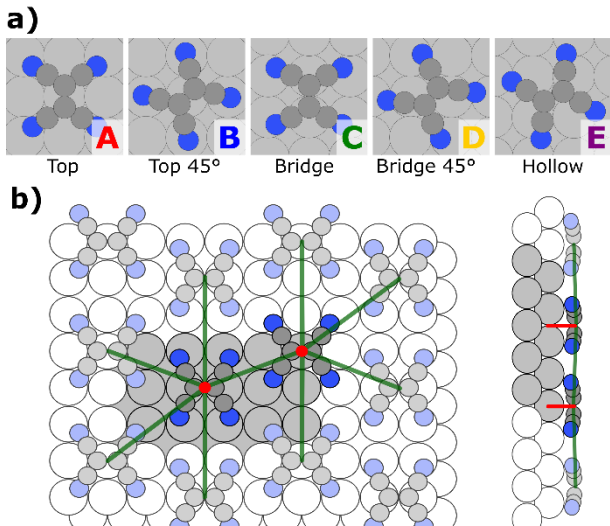


Figure 1: Strategy for structure prediction. a) Local adsorption geometries of TCNE/Ag(100) form the basic building blocks. b) Polymorphs are assembled as combinations of building blocks. Their energies are modelled as interactions with the substrate (red) and pairwise interactions between molecules (green).

Secondly, we use these *local adsorption geometries* (and the geometries that are symmetry equivalent by rotation, inversion and translation) on the substrate as building blocks to assemble larger structures containing multiple molecules/UC (Fig. 1b). This is effectively done by listing all possible combinations of all *local adsorption geometries* on all possible adsorption sites within a given supercell where the molecules do not collide, i.e. are farther apart than a given threshold ($d_{min} = 2.6 \text{ \AA}$). This procedure eliminates unphysical structures and allows a unique, exhaustive enumeration of the many potential energy minima. We note that for our example of TCNE/Ag(100), we find approx. 200.000 possible polymorphs containing up to 8 molecules/UC (see below). Thus, we have only reduced the search space from “completely intractable” to “still too many to be sampled exhaustively”.

While this discretization is already useful for finding the ground state structure when combining it with stochastic optimization methods¹⁴, here we want to explore the entire polymorphism. For this we need an efficient and accurate energy model instead. Here, it is possible to rely on a simple model, where the formation energy of any structure is given by two sets of energies: Interactions of the molecules with the substrate and interactions between the molecules, as depicted in Fig. 1b. For the molecule-substrate-interaction we introduce one parameter U_i per *local adsorption geometry*. For the molecule-molecule-interaction we assign one energy V_p to every possible pairwise interaction between molecules within a certain cutoff radius r_{max} . If these effective energies were known, the energy of any configuration could be determined by counting the

number of occurrences n_i of each local geometry and the number of occurrences n_p of each pairwise interaction:

$$E_{config} = \sum_{mol\ i} n_i U_i + \sum_{pairs\ p} n_p V_p \quad (1)$$

The challenge in determining the parameters is that even for modest cutoff radii r_{max} there are several thousand relevant pairwise interactions V_p .

In principle, one could calculate the interactions V_p directly by performing DFT calculations for all pairs of molecules, but this is impractical for several reasons: Foremost, the number of relevant pairs is very large, requiring immense computational effort. It has been tried to circumvent this problem by calculating only some of the pairwise interactions and use machine learning to predict the rest.⁶ However, there are two more issues: First, large supercells are required to decouple each pair from its periodic replicas, making every single DFT calculation very expensive. Secondly, the interactions obtained in this way may differ from the interactions within the system one is ultimately interested in. For instance, in a closed-packed structure, depolarization decreases the electrostatic repulsion between two charged molecules²².

We circumvent all these issues by not calculating the interactions directly, but rather inferring them from calculations of the actual, closely-packed metal/organic interface. This makes our parametrization simultaneously more accurate and computationally cheaper. Given enough instances of configurations with known energies E_{config} one could invert Eq. 1 and obtain the interactions U_i and V_p . This would still require at least m DFT calculations to determine m fit coefficients, where m is dominated by the number of included pairwise interactions which can be very large. To reduce the computational effort, we use a three-fold strategy:

First, we include *prior* knowledge about our fit-coefficients: Since we obtained the geometries of the isolated molecules with DFT in the first step of the SAMPLE approach, we already know their individual adsorption energies. These are used as educated guess for the U_i . Unfortunately, no comparable information exists about the interactions V_p . Since the interactions may be attractive or repulsive, it is most prudent not to assume anything about them. The starting point of our machine learning, therefore, is to assume that E_{config} is given by a non-interacting superposition of individual molecules.

Although we do not have prior knowledge about any specific V_p , we can make two general assumptions about

the set of V_p s as a whole: Interaction strengths tend to decrease with longer distances and "similar" pairs of molecules have similar interaction energies. Similarity between pairs of molecules is defined via the distance between suitable feature vectors for each pair of molecules: For this work, we use a sorted list of inter-atomic distances as feature vector.

These very general assumptions are encoded using the framework of Gaussian Process Regression by specifying a prior probability distribution for the interaction energies. Combining this prior distribution with the results of selected DFT calculations yields the posterior distribution for the interaction energies as outlined in the supporting information, while reducing the necessary number of training samples by an order of magnitude compared to other machine-learning approaches.

The second part of our strategy acknowledges the fact that not all configurations carry the same amount of information: Calculating different configurations that consist of the same or similar interactions creates mostly redundant information, which is a potential waste of computing time. Therefore, we additionally improve our prediction accuracy by systematic selection of the training dataset to provide a maximum of complimentary information. This can be achieved by selecting the training samples in such a way that the uncertainty of the posterior distribution of interactions is minimized. To minimize this uncertainty, we use Fedorov's algorithm²³ to select a d-optimal set of polymorphs for training. Since this set depends only on the chosen model and the prior assumptions, the training set can be selected as a whole before performing any calculations, allowing all DFT calculations to be run in parallel.

The third part of our strategy is based on the fact that not all data points are equally costly to acquire. For a given coverage, systems with fewer molecules/UC are modelled in smaller unit cells. On a formal basis, DFT scales with the number of electrons in the system cubed²⁴ and even in practice the scaling is somewhat worse than linear^{15,25}. The overall effort can thus be greatly reduced by preferentially sampling systems with a high translational symmetry, which can be modelled in small unit cells, even if the information gain per calculation is smaller.

Benchmarking the Machine Learning Model. To demonstrate the performance of this approach, we apply it to TCNE on Ag(100). This system shows an interesting peculiarity: It has high translational symmetry in one direction, but kinks and periodicities of varying length in the other²⁶ (Fig. 4a).

However, before tackling the actual system of interest, we need to ask two key questions: What prediction accuracy can we obtain? And: Is it indeed possible to predict the energies of large unit cells by training the model only on cheaper, smaller ones? To answer these questions, we first benchmark our approach on a well-controlled test system where an extensive dataset of DFT calculations can be readily obtained. For this, we consider a hypothetical TCNE monolayer without the substrate, but using the same polymorphs candidates that would also be obtained on the Ag(100) surface. When generating a list of all possible configurations that have the experimentally observed coverage (see Methods Section), we find 251 "small" configurations that contain 2 or 4 molecules/UC, and approximately 2×10^5 "large" configurations containing 6 or 8 molecules/UC.

To reliably assess the performance of our approach, we compiled a reference set that consists of all polymorphs with 6 or fewer molecules/UC, plus 2000 polymorphs drawn randomly from all polymorphs with 8 molecules/UC. The total energies of all ≈ 6000 of these geometries were calculated using DFT. As discussed in the next paragraphs, we then trained our model on various systematically selected subsets of this dataset to assess its predictions for various training set selections.

Fig. 2 shows the performance of the model for various numbers of training samples. In Fig. 2a, the model has seen very few training data, i.e. only 8 polymorphs with 2 molecules per cell and 10 polymorphs with 4 molecules per cell. It is therefore still biased towards the initial, non-interacting *prior* guess. Training on these 18 DFT calculations yields a Root Mean Square Error (RMSE) of 26 meV/molecule. Fig. 2b shows the prediction when including only a few more calculations on configurations with 4 molecules per cell (108 in total). It is particularly noteworthy that even though the model has been trained only on some of the small configurations, it gives not only excellent prediction accuracy for similar, small configurations (RMSE = 2.6 meV/molecule), but also yields good accuracy for the datasets with large configurations which it has never been trained on (RMSE = 12 meV/molecule). Since we have performed exhaustive DFT calculations for this model system, we can also confirm that there are no significant outliers (maximum deviation 68 meV). Additionally including a few large configurations into the training set (Fig. 2c) yields a RMSE of 4 meV/molecule across the entire dataset. We emphasize that these energy uncertainties are significantly lower than $k_B T$ at 300K (= 25 meV), or

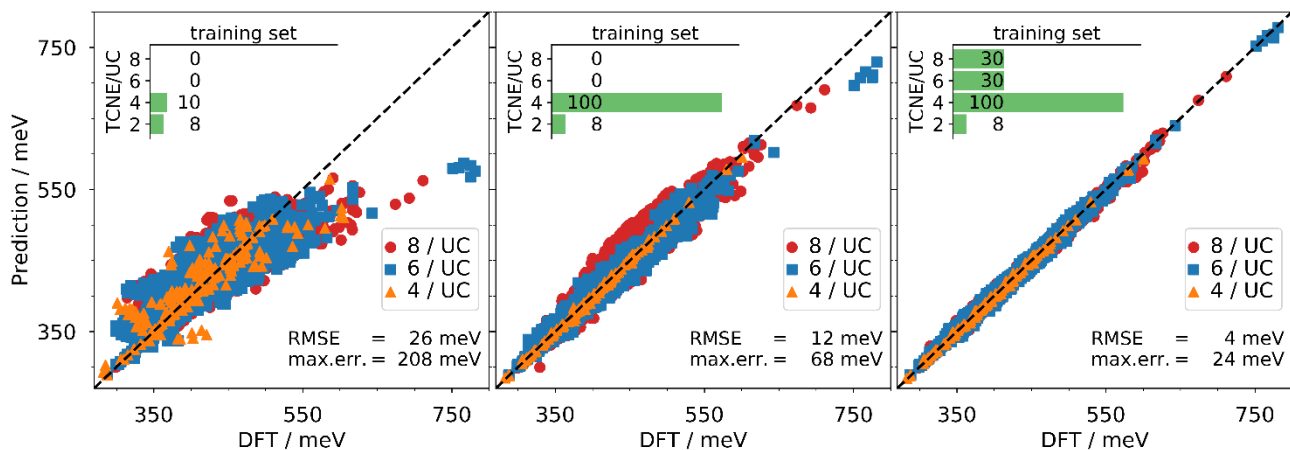


Figure 2: Comparison between the adsorption energies predicted by the machine learning model and the DFT reference calculations for varying training set sizes for the model system of a free-standing TCNE monolayer. Test points are colored according to the number of molecules within the unit cell. Inset: Number of training samples chosen from each unit cell size.

the often quoted "chemical accuracy" of 1 kcal/mol (43 meV) and are even within the numerical accuracy of our DFT calculations, which is approximately 10 meV (see Method Section). Our model is thus indeed able to predict energies with the same accuracy as DFT after having been trained only on 100-200 calculations, which is much more efficient than comparable approaches.²⁷⁻³⁰ Since these calculations preferentially include small unit cells that are computationally cheap, while still allowing predictions of larger, significantly more expensive calculations, the computational effort is reduced by 3-4 orders of magnitude compared to exhaustively calculating all polymorphs.

Application to TCNE/Ag(100). To predict the potential energy landscape of TCNE on Ag(100) the same training strategy was employed. Here, of course, computing an exhaustive dataset is prohibitively expensive. Therefore, we performed DFT calculations for 108 polymorphs with small unit cells: 8 polymorphs with 2 TCNE/UC and 100 polymorphs with 4 TCNE/UC. After training the model on this small dataset the formation energies for all other 2×10^5 configurations were predicted, allowing a ranking of the configurations according to their predicted formation energies as depicted in Fig. 3. Calculating all these formation energies with DFT would have

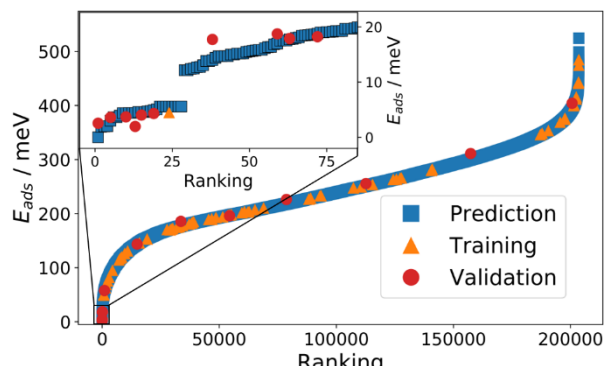


Figure 3: Ranking of configurations by predicted formation energies. The inset shows a zoom into the lowest 25 meV. More than 100 configurations lie within this energy range.

consumed about 1 million CPU-years on a BlueGene/Q cluster, while calculating the training set required only 0.002% of that effort. Additional validation calculations show a low RMSE of 6 meV/molecule across the entire energy range and 2 meV/molecule in the important low energy region. This accuracy is again well within the numerical accuracy of the underlying DFT calculations of approximately 10 meV.

Having finally obtained a comprehensive list of polymorph energies at DFT accuracy, we can now determine the global minimum (Fig. 4b): The structure that is predicted to be lowest in energy contains 6 TCNE/UC and consists of diagonal lines of molecules alternating between *top* and *bridge* positions. We note that only 2 of these molecules are inequivalent, as the same structure can also be described as a monoclinic unit cell containing 2 molecules. The fact that we could correctly find and predict the corresponding rectangular supercell, which is three times as large, is a further sign of the capability of our approach to deal with the vast configurational space.

Most importantly, we find that there are about 100 configurations within 25 meV/molecule of the predicted global minimum. This suggests that a large variety of different structures are present at room temperature (where the sample has been prepared) due to thermal excitation. It furthermore corroborates the importance to systematically sample low-energy structures beyond the global minimum. We note that some aspects of our ground-state structure do not comply with the experimental interpretation provided in ref. 26, as discussed in detail in the Supporting Information. While the origin of this discrepancy might be ascribed to kinetic trapping or deficiencies of the underlying electronic structure method, it does not compromise the efficiency of our machine-learning approach, which truthfully reproduces the DFT PES. Moreover, it is interesting to note that all of the energetically low-lying

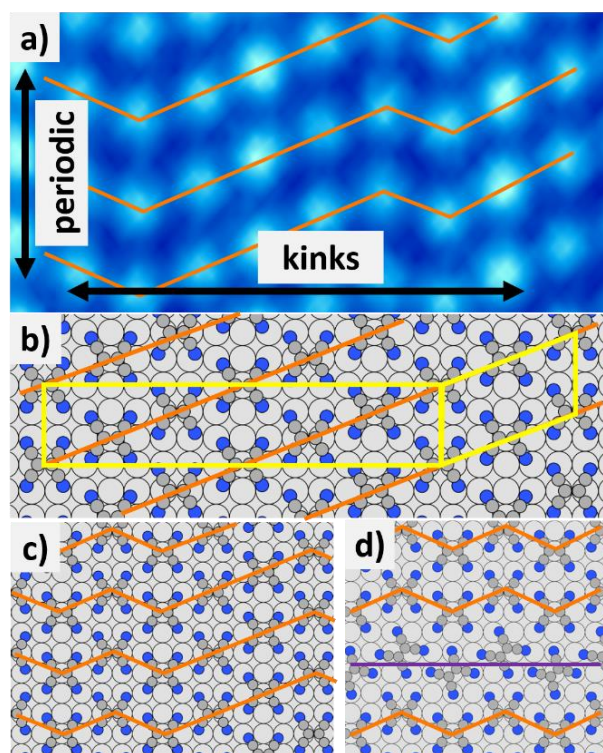


Figure 4: Exemplary structures predicted by the machine learning approach a) STM image of TCNE/Ag(100) courtesy of Daniel Wegner: Molecules form diagonal lines with strong periodicity in one direction, but frequent kinks in the other direction. b) Computed groundstate: Diagonal lines of molecules, alternating between top and bridge sites. Monoclinic unit cell and rectangular unit cell are marked in yellow. c) Kinks in the diagonal lines are low energy defects (4 meV/TCNE). d) Breaking the periodicity perpendicular to the lines is a high energy defect, requiring 120 meV/TCNE in the defect line.

structures that we find are variation of the ground-state structure, in particular kinks along the diagonal lines (Fig 4c) at various positions. No other defects with comparably low formation energies exists: Breaking periodicity in the high symmetry direction by introducing a line of inequivalent molecules (Fig. 4d) has an energetic cost of 120 meV per molecule in the line. This may explain why experiments find strong periodicity in one direction but random kinks in another direction (Fig 4a).

Summary. We have developed a machine learning model to predict the formation energies of organic monolayers. Training our model on as few as 100 DFT calculations of small periodic systems enables us to make predictions for arbitrarily large unit cells with DFT accuracy, enabling an extensive overview of the potential energy surface. Although our method is not necessarily cheaper than established structure search methods, it provides more relevant information (such as defect energies) for the same cost. We see applications in a large variety of surface science problems, in particular for structure search, study of polymorphs and defects. Including information about transition barriers

would make this model well suited for Monte Carlo studies of growth and surface dynamics due to its high accuracy at small computational cost.

We gratefully acknowledge Daniel Wegner for supplying experimental data and helping with their interpretation. We thank Egbert Zoer, Andreas Jeindl, and Matthias Rupp for fruitful discussions. Financial support by the Austrian Science Fund (FWF): P28631-N36 is gratefully acknowledged. The computational studies presented have been achieved using the Vienna Scientific Cluster (VSC) and the Argonne Leadership Computing Facility (ALCF), which is a DOE Office of Science User Facility supported under Contract DE-AC02-06CH11357.

References

- (1) Djuric, T.; Ules, T.; Flesch, H.-G.; Plank, H.; Shen, Q.; Teichert, C.; Resel, R.; Ramsey, M. G. *Cryst. Growth Des.* **2011**, *11*, 1015–1020.
- (2) Crispin, X.; Geskin, V.; Crispin, A.; Cornil, J.; Lazzaroni, R.; Salaneck, W. R.; Brédas, J.-L. *J. Am. Chem. Soc.* **2002**, *124*, 8131–8141.
- (3) Jorgensen, W. L. *Science* **2004**, *303*, 1813–1818.
- (4) Oganov, A. R. John Wiley & Sons, 2011.
- (5) L. Price, S. *Chem. Soc. Rev.* **2014**, *43*, 2098–2111.
- (6) Packwood, D. M.; Han, P.; Hitosugi, T. *Nat. Commun.* **2017**, *8*, ncomms14463.
- (7) Krautgasser, K.; Panosetti, C.; Palagin, D.; Reuter, K.; Maurer, R. J. *Chem. Phys.* **2016**, *145*, 84117.
- (8) Todorović, M.; Gutmann, M. U.; Corander, J.; Rinke, P. *ArXiv170809274 Cond-Mat* **2017**.
- (9) Panosetti, C.; Krautgasser, K.; Palagin, D.; Reuter, K.; Maurer, R. J. *Nano Lett.* **2015**, *15*, 8044–8048.
- (10) Nyman, J.; Day, G. M. *CrystEngComm* **2015**, *17*, 5154–5165.
- (11) Sojka, F.; Meissner, M.; Yamada, T.; Munakata, T.; Forker, R.; Fritz, T. J. *Phys. Chem. C* **2016**, *120*, 22972–22978.
- (12) Rodríguez-Fernández, J.; Lauwaet, K.; Herranz, M. Á.; Martín, N.; Gallego, J. M.; Miranda, R.; Otero, R. J. *Chem. Phys.* **2015**, *142*, 101930.
- (13) Reilly, A. M.; Tkatchenko, A. *Phys. Rev. Lett.* **2014**, *113*, 55701.
- (14) Obersteiner, V.; Scherbela, M.; Hörmann, L.; Wegner, D.; Hofmann, O. T. *Nano Lett.* **2017**, *17*, 4453–4460.
- (15) Blum, V.; Gehrke, R.; Hanke, F.; Havu, P.; Havu, V.; Ren, X.; Reuter, K.; Scheffler, M. *Comput. Phys. Commun.* **2009**, *180*, 2175–2196.
- (16) Perdew, J. P.; Burke, K.; Ernzerhof, M. *Phys. Rev. Lett.* **1996**, *77*, 3865–3868.
- (17) Tkatchenko, A.; DiStasio, R. A.; Car, R.; Scheffler, M. *Phys. Rev. Lett.* **2012**, *108*, 236402.

- (18) Ruiz, V. G.; Liu, W.; Zojer, E.; Scheffler, M.; Tkatchenko, A. *Phys. Rev. Lett.* **2012**, *108*, 146103.
- (19) Schuler, B.; Liu, W.; Tkatchenko, A.; Moll, N.; Meyer, G.; Mistry, A.; Fox, D.; Gross, L. *Phys. Rev. Lett.* **2013**, *111*, 106103.
- (20) Hofmann, O. T.; Atalla, V.; Moll, N.; Rinke, P.; Scheffler, M. *New J. Phys.* **2013**, *15*, 123028.
- (21) Deilmann, T.; Krüger, P.; Rohlfing, M.; Wegner, D. *Phys. Rev. B* **2014**, *89*, 45405.
- (22) Romaner, L.; Heimel, G.; Zojer, E. *Phys. Rev. B* **2008**, *77*, 45113.
- (23) Miller, A. J.; Nguyen, N.-K. *J. R. Stat. Soc. Ser. C Appl. Stat.* **1994**, *43*, 669–677.
- (24) Jensen, F. 2nd ed.; JW: Chichester, England ; Hoboken, NJ, 2011.
- (25) Hafner, J. *J. Comput. Chem.* **2008**, *29*, 2044–2078.
- (26) Wegner, D.; Yamachika, R.; Zhang, X.; Wang, Y.; Crommie, M. F.; Lorente, N. *Nano Lett.* **2013**, *13*, 2346–2350.
- (27) Rupp, M.; Tkatchenko, A.; Müller, K.-R.; von Lilienfeld, O. A. *Phys. Rev. Lett.* **2012**, *108*, 58301.
- (28) Behler, J. *Phys. Chem. Chem. Phys.* **2011**, *13*, 17930–17955.
- (29) Bartók, A. P.; Payne, M. C.; Kondor, R.; Csányi, G. *Phys. Rev. Lett.* **2010**, *104*, 136403.
- (30) Faber, F. A.; Hutchison, L.; Huang, B.; Gilmer, J.; Schoenholz, S. S.; Dahl, G. E.; Vinyals, O.; Kearnes, S.; Riley, P. F.; von Lilienfeld, O. A. *ArXiv170205532 Phys.* **2017**.

Supplementary Information to

Leaving the Valley: Charting the Energy Landscape of Metal/Organic Interfaces via Machine Learning

Michael Scherbela, Lukas Hörmann, Veronika Obersteiner, and Oliver T. Hofmann.

*Institute of Solid State Physics, NAWI Graz, Graz University of Technology,
Petersgasse 16, 8010 Graz, Austria*

1 Computational Methods

We used a 6 layer silver slab with a lattice constant of 3.94 Å for all surface calculations with a modified “tight” basis-set (removing Ag 5g and 4d basis functions) and an integration grid radial multiplier of 1. Our k-points were converged to a density of 24 k-points for the primitive Ag unit cell and scaled accordingly for larger unit cells. The geometry optimizations for the *local adsorption geometries* were done in a 6x6 supercell using the Broyden-Fletcher-Goldfarb-Shanno algorithm until the remaining forces were less than 0.01 eV/Å. All adsorption energies for multi-molecule configurations were obtained by single-point calculations. The machine learning was done using a custom python code using numpy, scipy and spglib. Visualizations were obtained using matplotlib and ASE.

For this study, we focus on the experimentally observed coverage for TCNE/Ag(100) of 59 Å²/molecule. However, we emphasize that this is not a necessary input, since it could, in principle, also be independently determined by determining polymorphs for various coverages and finding the one with the lowest Gibb’s energy per area²⁴. Furthermore, for this study we limit our search to rectangular unit cells of arbitrary size, for a simple technical reason: It allows us to systematically scale the k-point density and exploit equivalent k-points in (almost) all calculations, thus keeping the calculations numerically consistent. This facilitates the benchmark of the machine-learning model, which would be non-trivial when dealing with oblique unit cells.

2 Exemplary Structures generated by the SAMPLE procedure

Figure 1 shows a few exemplary configurations that are generated by the SAMPLE approach. They vary from strongly ordered to almost disordered structures.

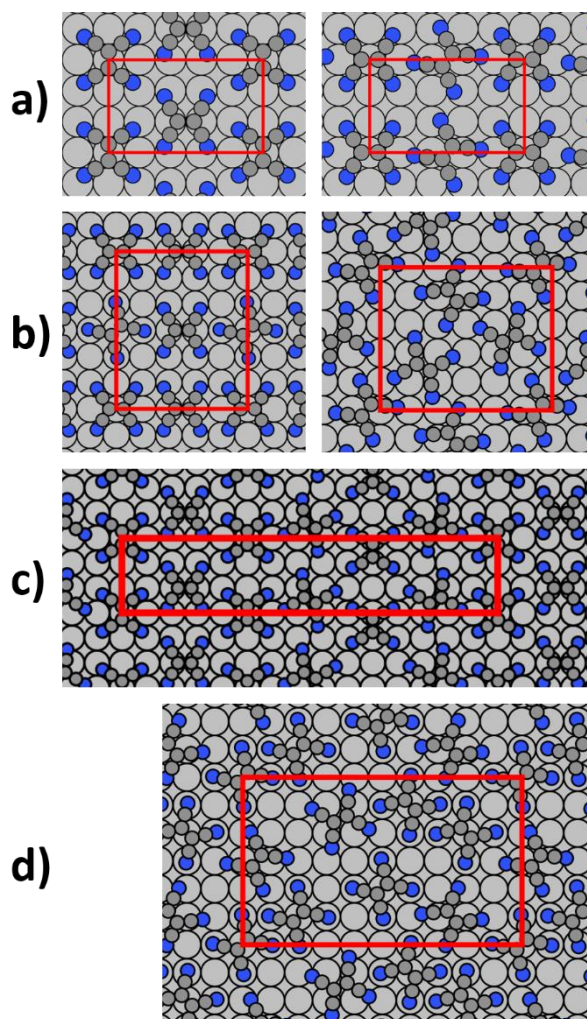


Figure 1 | Exemplary configurations generated by the SAMPLE approach for TCNE/Ag(100) in different unit cells and unit cell sizes. a) 2 TCNE per unit cell b) 4 TCNE/UC c) 6 TCNE/UC d) 8 TCNE/UC

3 Prior Covariance for Interactions

To determine the most likely interaction values we use a form of Gaussian Process Regression.

We specify an initial (noninteracting) guess μ for the interaction energies ω and a covariance matrix C for the corresponding uncertainties. The diagonal elements of

C encode the assumption of small interactions at long range, the off-diagonal elements encode correlations between similar pairs of molecules. This leads to a regularized fit for the interaction energies ω :

$$\begin{aligned} A\omega &= C^{-1}\mu + N^T E_{DFT}/\gamma^2 \\ A &:= C^{-1} + N^T N/\gamma^2 \end{aligned}$$

Here E_{DFT} is a vector of calculated energies for a list of configurations and N is a matrix that contains one row for each calculated configuration, specifying how often each interaction contributes within this configuration. The parameter γ specifies the (typically small) uncertainty of the DFT calculations, i.e. how far the calculations are expected to deviate from a fully converged result. For this work we used $\gamma = 5 \text{ meV}$. Solving this system yields the interaction energies ω and thus allows to predict the energy of any arbitrary configuration

Our initial guess for the interaction energies between molecules is non-interacting ($V_p = 0$). This guess is good when the molecules are well separated (and thus do indeed have little interactions) and is poor when the molecules are very close. We encode this varying certainty about our initial guess as a different variance C_{pp} for different pairs of molecules depending on their minimal separation d . For the prediction of TCNE/Ag(100) we used a maximal uncertainty $\sigma_{pairs} = 100 \text{ meV}$ at a minimal distance $d_{min} = 2.6 \text{ \AA}$ and an interaction decay-length of $\lambda = 5.0 \text{ \AA}$.

$$\sqrt{C_{pp}} = \sigma_{pairs} e^{-\frac{d-d_{min}}{\lambda}}$$

The covariance between two pairs of molecules i, j is determined by the similarity of their feature vectors v_i, v_j . To measure the distance between feature vectors the L1 norm was chosen. The degree of similarity up to which pairs of molecules are strongly correlated is determined by the hyperparameter α which was chosen to be 0.3 for feature vectors normalized to the interval $[0,1]$.

$$C_{ij} = \sqrt{C_{ii}C_{jj}} e^{-\frac{\|v_i-v_j\|_1}{\alpha}}$$

The hyperparameters α, λ and σ_{pairs} were chosen by physical intuition and confirmed to work well by cross validation. Prediction accuracy might be further improved by optimizing these hyperparameters, but we found no significant improvements in prediction accuracies when varying these parameters within physically reasonable ranges.

For the feature vector v we used a sorted list of interatomic distances, raised to a negative power. For our system we only considered the distances between nitrogen atoms of two TCNE molecules, since they form the cornerstones of the molecule:

$$v = \begin{pmatrix} d_1^{-2} \\ d_2^{-2} \\ \vdots \end{pmatrix}$$

4 D-optimal training set selection

To demonstrate the power of d-optimal training set selection we trained the model on 1000 randomly selected training sets (each containing 48 configurations) from the TCNE/vacuum test system and recorded its Root Mean Square Error (RMSE) on a validation set. Fig. 2 shows the distribution for these 1000 RMSE values compared to the RMSE of a d-optimally selected training set. The d-optimally selected set outperformed the random selection in 97% of all trials and gave a RMSE of 13 meV while the randomly selected test sets had a mean RMSE of 18 meV.

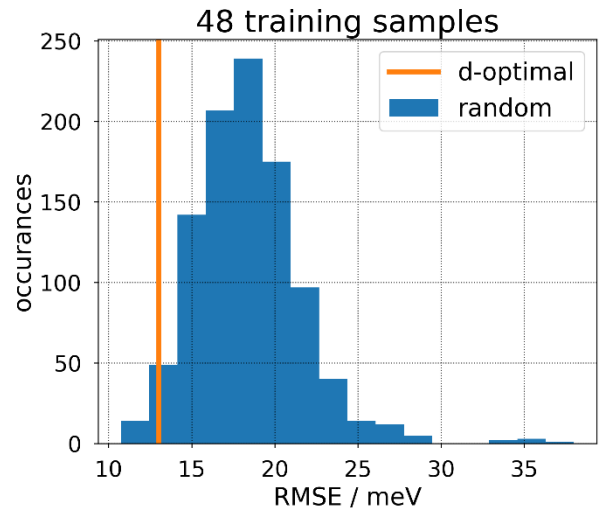


Figure 2 | Root Mean Square Error (RMSE) distribution for randomly selected training sets compared to the RMSE obtained by D-optimal training set selection. D-optimal selection beats random selection in 97% of trials and decreases the mean prediction error by about 30% at no additional computational cost.

5 Similarities and Differences to Cluster Expansion

While our method shares some similarities with a truncated Cluster Expansion (CE), it has several features that clearly distinguish it: In a CE - often used for inorganic crystals - the number of fit coefficients is typically significantly larger due to the inclusion of higher-order clusters and must be reduced by meta-optimizations such as Genetic Algorithms²⁵ or by enforcing sparseness as a regularization via compressed sensing²⁶. In contrast, organic monolayers - consisting of larger, more complex building blocks - are less dependent on contributions beyond pairwise interactions (see ref 12) but show no signs of a sparse distribution of interactions. However, the interaction energies in organic monolayers are correlated between similar pairs of molecules, enabling a significant reduction of the number of training calculations compared to a naïve CE.

6 PBEsol dataset

To show that the method is transferrable between different methodologies, in addition to PBE we also obtained the potential energy surface (PES) for TCNE/Ag(100) using the PBEsol exchange-correlation functional. PBEsol yields a significantly different PES, in particular because it destabilizes the *local adsorption geometry A* ("top") relative to the other *local adsorption geometries*.

Nonetheless the machine learning model can just as well reproduce the results obtained by the PBEsol functional when trained on PBEsol calculations. Fig. 3 shows the predictions for a validation set after having trained the model on 68 configurations. Just as for the PBE dataset, also for PBEsol the prediction accuracy is high with a Root Mean Square Error of 12 meV.

7 Differences between Prediction and Experiment

When comparing our predicted ground-state structure

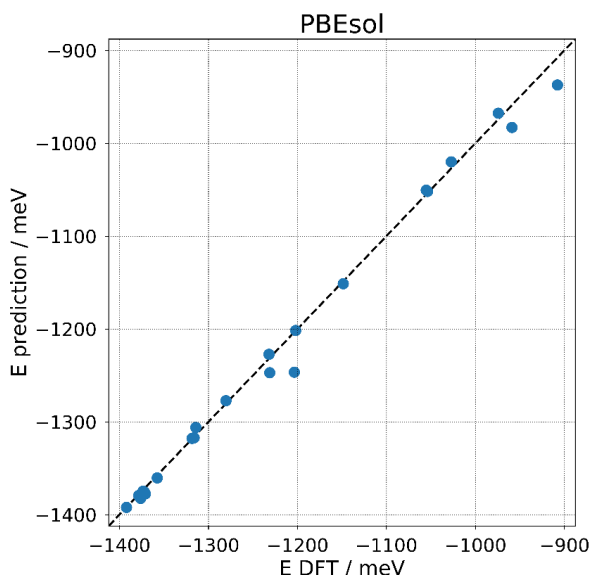


Figure 3 | Prediction accuracy for the PBEsol dataset. Training the model on 68 DFT calculations yields a RMSE of 12 meV on this validation set and again no significant outliers. This underlines the transferability of the machine learning model between different methodologies.

to the experimental interpretation drawn from STM and STS measurements¹⁸, we find two notable differences: Experiments report up to four inequivalent molecules per unit cell: Of these, one molecule is clearly assigned to a "top" adsorption site and two are clearly positioned at a "bridge" site. The fourth molecule is more ambiguous, but tentatively also assigned a bridge position in ref 18. This is at clear variance with our DFT results, that find a *top/bridge* ratio of 1:1 to be energetically more favorable by 250 meV / molecule. A second apparent discrepancy is that in the STM images, every other molecule appears to be rotated by 90°. In contrast, our DFT calculation find parallel molecules to be energetically favorable by about 80 meV. The energy

differences are about one order of magnitude larger than our numerical accuracy. We want to stress that the discrepancies between experiment and theory are not a shortcoming of our machine learning model, but borne out from the underlying electronic structure theory.

7.1 Effect of the Methodology: Top vs Bridge

To investigate the difference in adsorption energy between the top and the bridge geometry in more detail we calculated the adsorption energy for an isolated molecule with different functionals. For all functionals we calculated the adsorption energy of a molecule sitting on either a top or a bridge position using the geometries obtained from PBE. The energy differences between top and bridge are listed in Tab. 1. When including the vdW^{surf} correction the top geometry is lower in energy by more than 200 meV compared to the bridge geometry, independent of the XC-functional used.

To estimate the influence of vibrational enthalpy we calculated the vibrational energy of both the *top* as well as the *bridge* adsorption geometry while keeping the positions of the substrate atoms fixed. The vibrational zero-point energy (ZPE) for the *top* geometry is 1.210 eV, the ZPE for the *bridge* position is 1.193 eV. The vibrational ZPE thus raises the adsorption energy of the *top* geometry by only 17 meV relative to the *bridge* geometry and can therefore not sufficiently destabilize the *top* adsorption geometry to account for the more frequent observation of bridge sites in experiment.

Table 1 | Difference in adsorption energy between the Bridge and Top adsorption geometry for different XC-functionals, including and excluding the impact of the vdW^{surf} correction. and optionally TS van der Waals correction.

| functional | with vdW / meV | without vdW / meV |
|------------|----------------|-------------------|
| PBE | 316 | 138 |
| HSE | 393 | 211 |
| PBEsol | 219 | 240 |
| revPBE | 249 | 65 |
| AM05 | 206 | 206 |
| SCAN | 224 | 224 |
| TPSS | 213 | 213 |

7.2 Effect of the Methodology: Parallel vs Orthogonal Molecules

To address the issue of orthogonal vs rotated molecules we calculated the energetic difference between both geometries for a polymorph with 2 molecules per unit cell with a variety of different methodologies. We always find that it is energetically favorable for the

molecules to align parallel, as opposed to aligning orthogonal to each other. We observe that this energetic difference is already present when considering a TCNE dimer in the gas-phase. Furthermore, this energetic ordering is independent from the exact positioning of the molecules relative to each other. Fig. 4 shows that for all positions of the TCNE molecules relative to each other the parallel arrangement is favorable compared to the orthogonal arrangement. We also investigated this energetic difference between parallel and rotated molecules in gas-phase for different methodologies as listed in Tab. 2. None of these changes significantly altered the energetic difference: All settings resulted in the parallel orientation to be favorable by about 50-60 meV.

Table 2 | Energetic difference between rotated and parallelly oriented molecules for different computational settings

| | parallel/eV | orthogonal/eV | Δ /meV |
|----------------------------|-------------|---------------|---------------|
| PBE | -24356.261 | -24356.202 | 59 |
| PBE large basis set | -24356.312 | -24356.253 | 59 |
| PBE + MBD | -24356.261 | -24356.202 | 59 |
| PBE0 | -24354.279 | -24354.222 | 57 |
| SCAN | -24372.308 | -24372.254 | 54 |

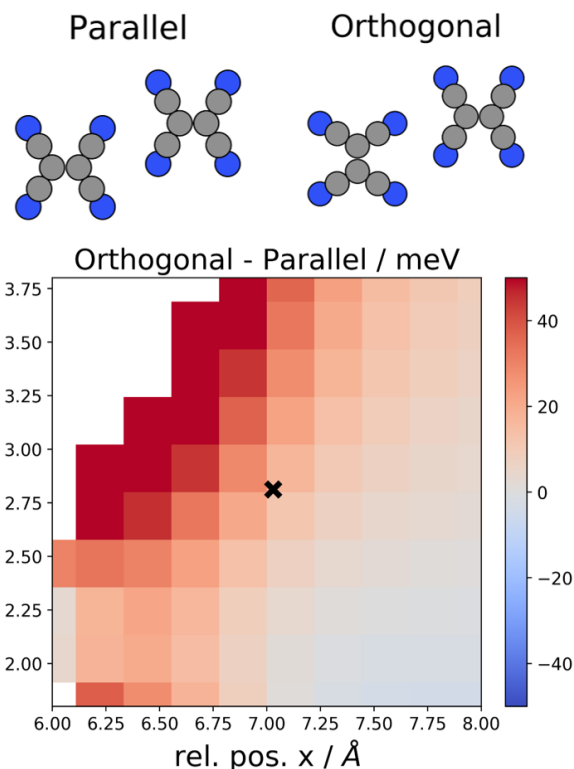


Figure 4 | Energetic difference between dimers of parallel and rotated molecules depending on the dimer separation. For all considered relative positions the parallelly oriented molecules are lower in energy compared to the orthogonally arranged molecules. The x marks the relative position in the periodic polymorph and the tests conducted in Tab. 2.